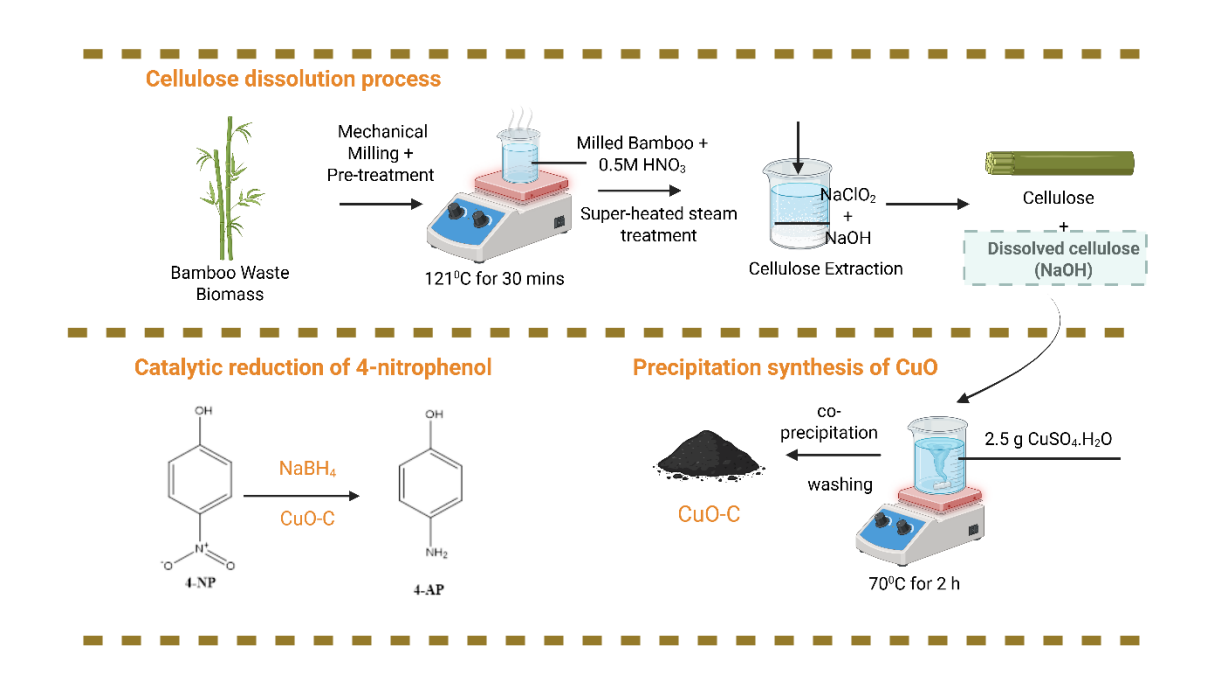
Synthesis of CuO Nanoparticles Using Waste-Derived Bamboo Cellulose for Enhanced Catalytic and Antibacterial Applications

Alvin Lim Teik Zheng , a,b* Sarah Sabidi , Melissa Alexander Maran, Tan Kar Ban , Kelly Wong Kai Seng , Eric Lim Teik Chung , and Yoshito Andou , h

*Corresponding author: alvinltz@upm.edu.my

DOI: 10.15376/biores.20.4.9148-9166

GRAPHICAL ABSTRACT



Synthesis of CuO Nanoparticles Using Waste-Derived Bamboo Cellulose for Enhanced Catalytic and Antibacterial Applications

Alvin Lim Teik Zheng , a,b,* Sarah Sabidi , Melissa Alexander Maran, Tan Kar Ban , Kelly Wong Kai Seng , Eric Lim Teik Chung , and Yoshito Andou , h

Copper oxide (CuO) nanoparticles were prepared using waste-derived cellulose from bamboo biomass as a functional additive. The cellulose, recovered from an alkaline dissolution process, enhanced the dispersion and structural integrity of CuO nanoparticles (NPs). The CuO prepared in the presence of waste cellulose (CuO-C) exhibited a specific surface area of 32 m²/g, compared to 7 m²/g for pure CuO. Scanning electron microscopy (SEM) revealed a feather-like CuO structure influenced by the presence of the waste-derived cellulose matrix. The catalytic activity of CuO-C was tested through the reduction of 4-nitrophenol (4-NP) to 4-aminophenol (4-AP), achieving complete conversion within 15 min. The synthesis cost of CuO-C was approximately RM 3.30 per gram. Antibacterial tests confirmed activity against both *Staphylococcus aureus* and *Klebsiella pneumoniae*. These findings demonstrate the feasibility of using a highly alkaline solution from the cellulose dissolution process to produce low-cost CuO with improved catalytic and antibacterial properties.

DOI: 10.15376/biores.20.4.9148-9166

Keywords: Copper oxide; 4-Nitrophenol; Cellulose; Waste management

Contact information: a: Institute of Ecoscience Borneo, Universiti Putra Malaysia Bintulu Campus, Bintulu 97008, Sarawak, Malaysia; b: Department of Science and Technology, Faculty of Humanities, Management and Science, Universiti Putra Malaysia Bintulu Campus, Bintulu 97008, Sarawak, Malaysia; c: Nuclear Medicine Department, Beacon Hospital Sdn. Bhd, No 1 Jalan 215 section 51, Off Jalan Templer, 46050 Petaling Jaya, Selangor, Malaysia; d: Department of Chemistry, Faculty of Science, Universiti Putra Malaysia, Serdang 43400 Selangor, Malaysia; e: Department of Agribusiness and Bioresource Economics, Faculty of Agriculture, Universiti Putra Malaysia, Serdang 43400, Malaysia; f: Department of Animal Science, Faculty of Agriculture, Universiti Putra Malaysia, Serdang 43400, Malaysia; g: Institute of Tropical Agriculture and Food Security, Universiti Putra Malaysia, Serdang 43400, Malaysia; h: Graduate School of Life Sciences and Systems Engineering, Kyushu Institute of Technology, Fukuoka 808-0196, Japan; *Corresponding author: alvinltz@upm.edu.my

INTRODUCTION

The increasing demand for sustainable and efficient materials has driven significant research interest in the development of nanostructured catalysts for environmental and industrial applications. Among various candidates, copper oxide (CuO) has emerged as a highly promising material due to its unique physicochemical properties, including high surface reactivity, thermal stability, and semiconducting behavior (Tran and Nguyen 2014; Naz et al. 2023; Devaraji et al. 2024). CuO-based materials have been widely explored for applications such as catalysis (Poreddy et al. 2015; Zedan et al. 2018; Bhaskar et al. 2024), gas sensing (Wang et al. 2016; Steinhauer 2021; Bhat et al. 2023), photocatalysis (Raizada et al. 2020; Nazim et al. 2021; Sibhatu et al. 2022), and environmental remediation (Saif

et al. 2021; Chakrabarty et al. 2023). However, the scalability and economic feasibility of CuO synthesis remain critical challenges, necessitating innovative approaches that integrate cost-effective and sustainable resources.

Cellulose, the most abundant biopolymer on Earth, presents an attractive solution to these challenges. As a renewable and biodegradable material, cellulose has gained considerable attention for its ability to act as a structural and functional additive in nanomaterial synthesis (Mekhzoum *et al.* 2021; Kassie *et al.* 2024). Notably, waste-derived cellulose offers additional benefits, as it reduces environmental burden while providing a virtually cost-free raw material. Incorporating cellulose into CuO synthesis not only enhances the material's sustainability but also improves its textural and morphological properties, such as increased surface area and porosity (Zhou *et al.* 2013). Moreover, the use of structural additives such as cellulose during synthesis offers a sustainable pathway not only to control nanoparticle morphology but also to facilitate downstream recovery. Despite these advantages, the integration of waste-derived cellulose in the synthesis of CuO nanostructures has been underexplored.

Water pollution poses a significant threat to environmental sustainability and public health, with industrial activities being one of the primary contributors to the contamination of aquatic ecosystems. Among various pollutants, organic compounds such as 4-nitrophenol (4-NP) have garnered considerable attention due to their widespread use and toxicity (Zhao *et al.* 2010; Xu *et al.* 2024b). 4-NP, a priority pollutant identified by the United States Environmental Protection Agency (EPA), is commonly utilized in the production of pesticides, dyes, and pharmaceuticals. Its high solubility in water and resistance to natural degradation processes exacerbate its environmental persistence, leading to the contamination of surface and groundwater resources. The accumulation of 4-NP in water bodies poses severe risks to aquatic life and human health, as it is both carcinogenic and mutagenic at elevated concentrations (Panigrahy *et al.* 2022).

The catalytic reduction of 4-NP serves as a model reaction for evaluating the efficiency of nanostructured catalysts (Menumerov et al. 2016; Ehsani et al. 2023; Zheng et al. 2024). This reaction holds significant industrial relevance, as 4-AP is a key intermediate in the production of pharmaceuticals, dyes, and agrochemicals (Li et al. 2021). Traditionally, noble metals such as platinum (Pt) (Li et al. 2014; Xu et al. 2024a), palladium (Pd) (Jadbabaei et al. 2017; Su et al. 2016), silver (Ag) (Kästner and Thünemann 2016; Sudhakar and Soni 2018) and gold (Au) (Neal et al. 2019; Noël et al. 2020) have been employed as catalysts for the reduction of 4-NP due to their exceptional catalytic efficiency and stability. However, the high cost and limited availability of noble metals have hindered their large-scale application, prompting the search for cost-effective and sustainable alternatives. Previously, Bekru reported on CuO NPs synthesized via plant extract for 4-NP reduction (Bekru et al. 2021). CuO NPs synthesized using Cordia africana Lam. leaf extract exhibited a better reducing capacity with an activity parameter constant of 75.8 min⁻¹·g⁻¹. CuO/kaolin NC was also reported for demonstrated superior catalytic performance with high 4-NP conversion into 4-AP (Asmare et al. 2024).

This work presents a sustainable route to synthesize CuO using cellulose extracted from bamboo biomass waste. The alkaline solution retained from the cellulose extraction process is reused directly as the reaction medium for CuO precipitation. This strategy eliminates the need for purified cellulose or external templating agents, integrating waste valorization into the material design process. The reduction of 4-NP to 4-AP is employed as a model reaction to evaluate catalytic performance. Antibacterial properties are also assessed. Additionally, this work provides a cost analysis to demonstrate the economic

feasibility of this method. This study highlights the functional and economic benefits of coupling metal oxide synthesis with waste-derived biomass resources.

EXPERIMENTAL

Materials

Copper (II) sulfate pentahydrate (CuSO₄· $5H_2O$, $\geq 99.5\%$) and sodium hydroxide (NaOH, $\geq 97.0\%$) were purchased from Fujifilm Wako Pure Chemical Corporation, Japan. All reagents were used without further purification. Deionized water was used for all preparations.

Cellulose Extraction

Cellulose was extracted from bamboo biomass using a multistep pretreatment and hydrothermal process. The biomass was milled and boiled in 0.5 M nitric acid at 121 °C for 30 min to remove lignin and hemicellulose. The sample was then subjected to superheated steam at 265 °C for 5 min. The solid fraction was bleached with sodium chlorite and treated with 8.8 wt% NaOH to remove residual lignin. The recovered cellulose (degree of polymerization: 312) was filtered and dried. The alkaline solution retained from this process was stored for use in CuO synthesis. This combination of nitric acid boiling and alkaline extraction has been shown to remove up to 90% of lignin and a significant portion of hemicellulose, resulting in cellulose-enriched biomass suitable for further processing (Liu *et al.* 2020).

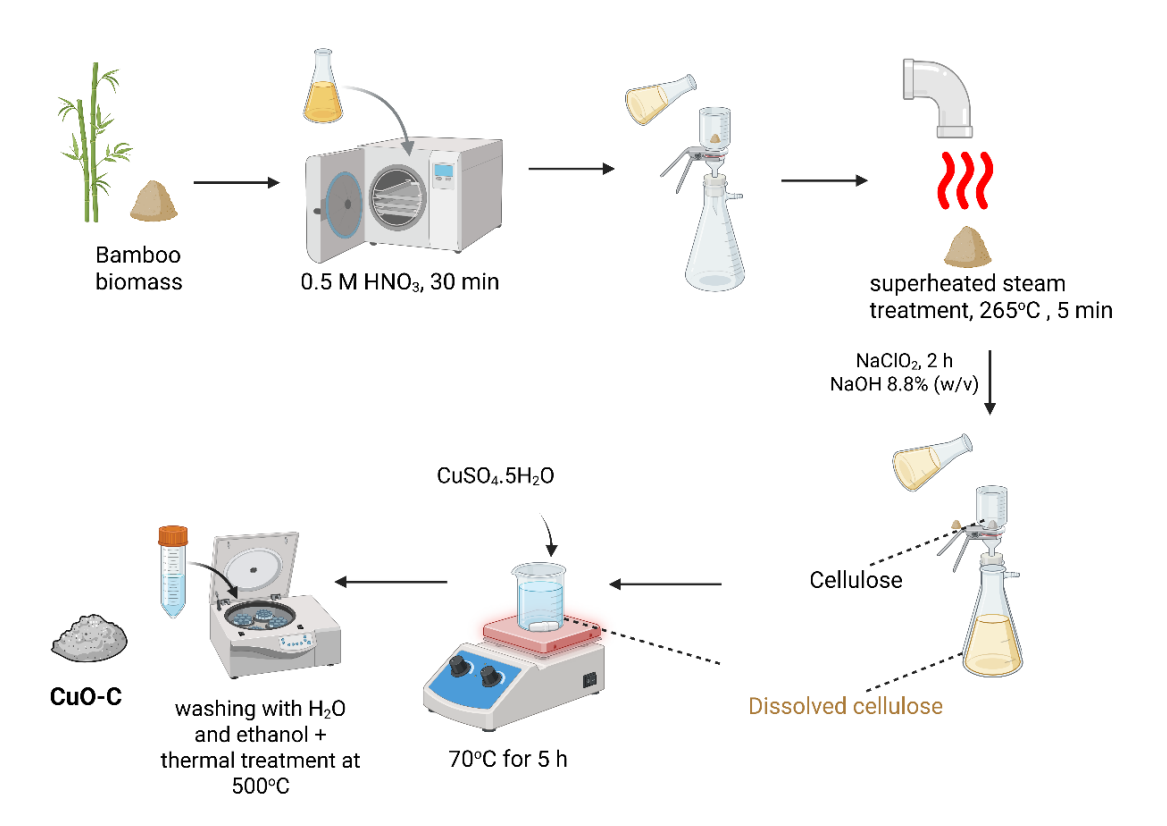


Fig. 1. Waste cellulose extraction procedure for the synthesis of CuO-C

Preparation of CuO and CuO-C

For CuO, 2.5 g of CuSO₄·5H₂O was dissolved in 100 mL of deionized water. A NaOH solution (1 g/mL) was added dropwise under vigorous stirring at 70 °C to initiate precipitation. For CuO-C, the cellulose-rich alkaline solution from the extraction step was used in place of deionized water and NaOH. The Cu precursor was added to this solution under identical stirring and temperature conditions. After reaction, the products were centrifuged at 4500 rpm for 15 min, washed with deionized water and ethanol, then dried at 70 °C for 24 h. Thermal treatment was performed at 500 °C for 2 h to remove residual cellulosic content.

Characterization

The CuO and CuO-C were characterized to assess their morphological, optical, structural, and chemical properties. Morphological analysis was performed using a JEOL 6000 scanning electron microscope (SEM) equipped with an energy-dispersive X-ray analyzer (EDX) operated at 10 kV accelerating voltage. Crystallographic structures were examined using a Rigaku X-ray diffractometer with Cu K-α radiation at 40 kV and 15 mA with a scan rate of 10°/min. ATR-FTIR spectra were recorded on a Nicolet iS5 spectrometer (Thermo Fisher Scientific, Wisconsin, USA) to analyze functional groups. Thermal stability was assessed using an EXSTAR TG/DTA7000 instrument (Hitachi High-Tech, Tokyo, Japan) under a continuous N₂ stream. Raman spectra were obtained with a JASCO NRS-5100 Laser Raman Spectrometer (JASCO International Co., Ltd., Tokyo, Japan) using a 532 nm excitation wavelength and a 2.5 mW laser power beam. Surface area and pore size distribution were calculated using N₂ adsorption-desorption isotherms and the DFT method on a Quantachrome Instruments Surface Area and Pore Size Analyzer (Boynton Beach, Florida, USA).

Catalytic Activity Test

The preliminary catalytic activities of CuO and CuO-C were evaluated using the reduction of 4-NP to 4-AP as a model reaction. The reaction was carried out in a flask containing 50 mL of 10 mg/L 4-NP solution. To this, 50 mg of NaBH4 and 10 mg of the catalyst were added. At regular intervals, 1 mL of the reaction mixture was sampled and diluted to 10 mL with deionized water. The progress of the reaction was monitored using a SHIMADZU UV-1800 spectrophotometer by measuring the absorbance of 4-NP at 401 nm. The reduction process was further verified by the appearance of a new absorption peak at 298 nm corresponding to 4-AP. To illustrate the time-resolved catalytic transformation, representative samples were taken at 2-minute intervals to observe the conversion of 4-NP to 4-AP.

Antibacterial Test

The antibacterial activity of CuO and CuO-C samples was evaluated against Staphylococcus aureus ATCC 6538P and Klebsiella pneumoniae using method reported previously (Zheng et al. 2022). A single bacterial colony was inoculated into 10 mL of Luria–Bertani (LB) broth and incubated overnight at 37 °C under aerobic conditions. Subsequently, 200 µL of the overnight culture was transferred to 20 mL of fresh LB broth and incubated at 37 °C until the optical density at 600 nm (OD600) reached approximately 0.5. The bacterial cells were then harvested by centrifugation at 13,000 rpm for 1 min, washed four times to remove residual growth medium, and diluted 1:50 in phosphate-buffered saline (PBS; 50 mM sodium phosphate, pH 7.5, containing 150 mM NaCl). The

CuO and CuO-C samples were dispersed in PBS containing 10⁶ CFU/mL bacterial suspension in sterilized conical flasks and incubated for 2 h at room temperature with shaking at 200 rpm. After incubation, serial 10-fold dilutions of the bacterial suspensions were prepared and plated onto LB agar using the spot test method. Bacterial growth was assessed by photographing the plates after overnight incubation at 37 °C, and colony-forming units (CFUs) were quantified using ImageJ software, with manual counting performed to validate the software results. Each experiment was conducted in triplicate, with three plates used per bacterial concentration.

RESULTS AND DISCUSSION

The XRD patterns of CuO and CuO-C are shown in Fig. 2(a). The XRD patterns confirmed the monoclinic phase of CuO for both samples, with peaks matching JCPDS card no. 48-1548. The observed peaks at 2θ values of approximately 32.5°, 35.5°, 38.7°, 48.7°, 53.6°, 58.3°, 61.5°, 66.3°, 68.1°, and 75.1° correspond to the (110), (111), (112), (202), (020), (113), (311), (220), (311), and (004) planes, respectively (Hong *et al.* 2009; Peng *et al.* 2020). The sharp and well-defined peaks indicate the high crystallinity of the synthesized CuO.

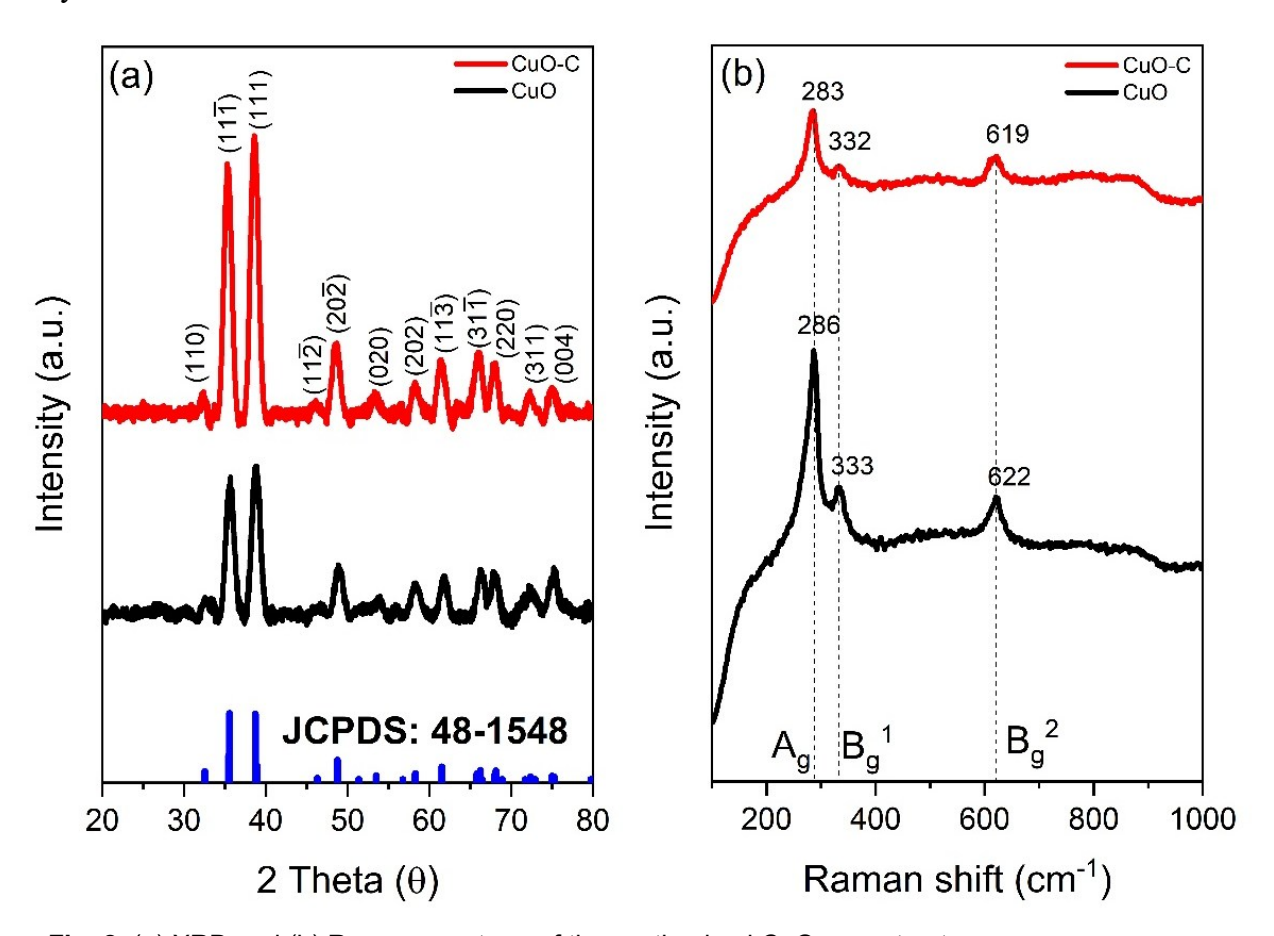


Fig. 2. (a) XRD and (b) Raman spectrum of the synthesized CuO nanostructures

For the CuO-C, the XRD pattern exhibits similar characteristic peaks of CuO, suggesting that the incorporation of cellulose does not alter the monoclinic crystal structure

of CuO. However, the slight broadening of the peaks and a marginal decrease in peak intensity in the CuO-C sample imply a reduction in crystallite size or partial amorphization due to the interaction with cellulose during crystal growth (Warren and LaJeunesse 2019). The Scherrer equation was employed to estimate the crystallite size using the full-width at half-maximum (FWHM) of the most intense diffraction peaks. The calculated crystallite size for pure CuO was found to be approximately 6.14 nm, while the crystallite size for the CuO-C was 7.18 nm. The larger crystallite size observed for CuO-C can be attributed to the stabilizing effect of the waste-derived cellulose, which prevents excessive NP agglomeration and maintains discrete NP structures.

The Raman spectra of CuO and CuO-C are presented in Fig. 2(b). The spectra for both samples exhibit distinct peaks characteristic of monoclinic CuO at approximately 283 cm⁻¹, 332 cm⁻¹, and 619 cm⁻¹ correspond to the vibrational modes Ag, Bg¹ and Bg² (Xu *et al.* 1999). In the CuO-C spectrum, a slight shift in the vibrational bands was observed. The shift in Raman peaks is caused by point-like lattice impurities in crystalline NPs (Koniakhin *et al.* 2024). This shift is indicative of an interaction between the Cu precursor and the waste-derived cellulose matrix, likely from hydrogen bonding or coordination interactions. The broadening of the Raman peaks in the CuO-C compared to pure CuO is consistent with the partial amorphization and reduced crystallite size inferred from the XRD results (Wang *et al.* 2012). This indicates that cellulose acts as a stabilizing agent, influencing the structural and vibrational properties of CuO NPs.

Figure 3(a) illustrates the N₂ adsorption-desorption isotherms of CuO and CuO-C, while Fig. 3(b) presents their pore size distributions obtained via Density Functional Theory (DFT) analysis. The isotherms for both samples exhibit type-IV characteristics with hysteresis loops, indicative of mesoporous structures (Shimizu and Matubayasi 2024). However, the CuO-C demonstrated a significantly higher adsorption volume compared to pure CuO, highlighting an enhanced surface area and porosity due to the influence of the waste-derived cellulose. The specific surface area (SSA) was 32 and 7 m²/g for CuO-C and CuO, respectively. This significant increase in SSA can be attributed to the inhibition of particle agglomeration and enhancement of the dispersion of CuO NPs. The cellulose likely serves as a structural template, creating additional surface area by forming interconnected pores and reducing particle aggregation (Ajiz *et al.* 2024). Consequently, the CuO-C benefits from improved textural properties, including enhanced porosity and surface area, which are advantageous for applications such as adsorption, catalysis, and environmental remediation. The average pore size further supports this observation, revealing a pore size of 3.1 nm for CuO and a slightly reduced size for CuO-C as shown in Table 1.

Table 1. SSA, Pore Volume and Pore Size Obtained for the CuO and CuO-C

Material	S _{вет} (m²/g)	Pore volume (cc/g)	Average pore size (nm)
CuO	7.33	0.035	3.10
CuO-C	31.62	0.148	2.84

The findings show that waste-derived cellulose likely prevented excessive particle aggregation while creating a more open structure during CuO formation, as evidenced by the significant increase in pore volume and surface area.

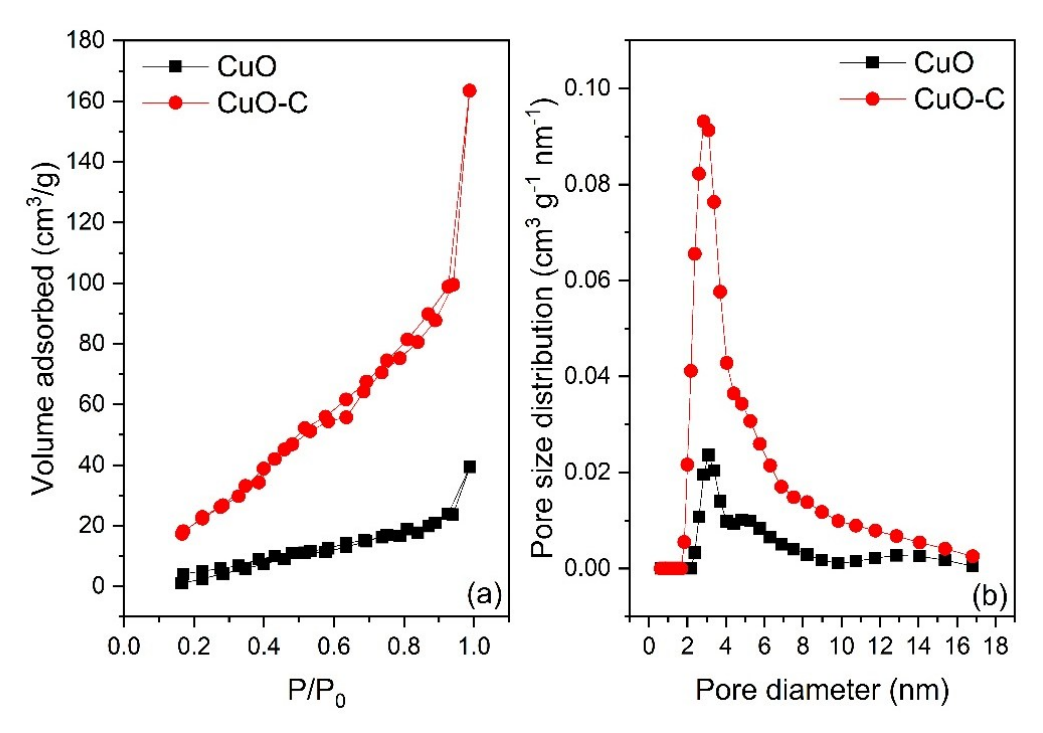


Fig. 3. (a) N₂ adsorption-desorption isotherm (b) DFT pore size distribution of the synthesized CuO nanostructures

The UV-DRS absorption spectra and Tauc plots for the CuO and CuO-C are shown in Fig. 4(a) and 4(b), respectively.

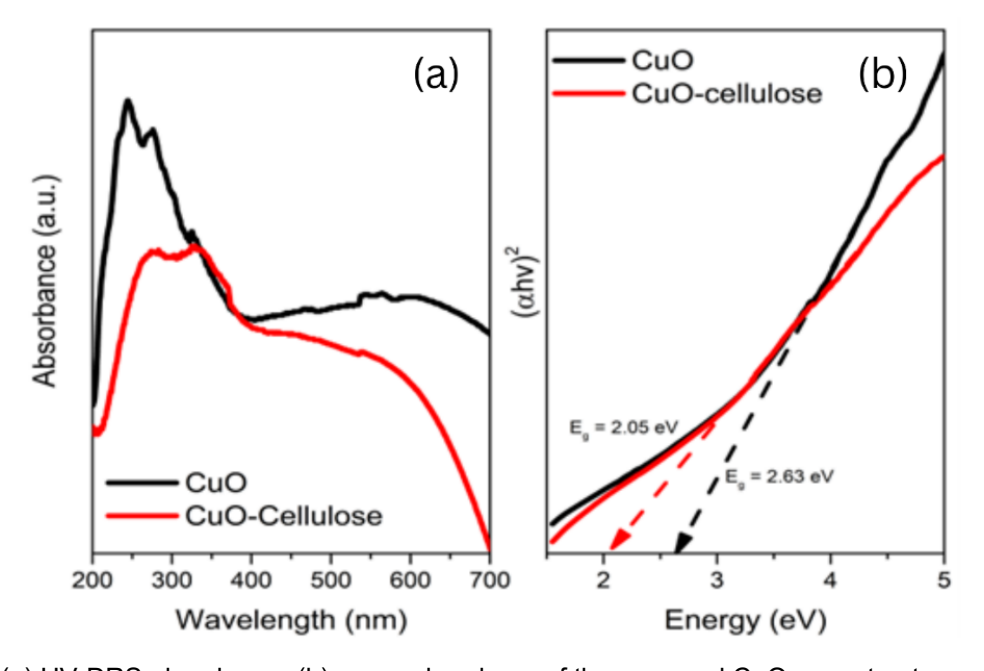


Fig. 4. (a) UV-DRS absorbance (b) energy band gap of the prepared CuO nanostructures

The absorbance spectrum of pure CuO exhibited a broad absorption band extending from the UV to the visible region, with a maximum absorbance edge around 272 nm. In contrast, the CuO-C showed a red-shifted absorbance edge, with enhanced absorption

intensity in the visible region. This shows that the waste-derived cellulose modified the electronic environment around the CuO NPs. The band gap energy (E_g) was estimated using the Tauc plot method. Pure CuO exhibited an E_g of 2.63 eV, confirming its semiconducting nature. The CuO-C sample showed a lower band gap of 2.05 eV. This reduction may have resulted from electronic interactions between CuO and the cellulose phase, which could introduce defect states, enhance carrier delocalization, or facilitate band tailing due to structural disorder during synthesis (Aggarwal *et al.* 2024).

The FTIR spectra of CuO and CuO-C are presented in Fig. 5(a). For pure CuO, the peaks at 3442 cm⁻¹ and 491 cm⁻¹ correspond to the stretching vibration of surface hydroxyl groups and Cu-O bonds, respectively (Mistry *et al.* 2024). In the CuO-C sample, the peak at 495 cm⁻¹ corresponds to the Cu-O bond and shows a slight shift, indicating hydrogen interaction between CuO and residual carbon. The absence of significant additional peaks in the CuO-C spectrum suggests that the waste-derived cellulose did not chemically alter the CuO NP. These interactions contribute to the stability and dispersibility of the CuO, enhancing its functional properties for various applications. Notably, the FT-IR further confirms that all cellulosic materials were removed during the thermal treatment process which supports the XRD result (absence of amorphous peaks for cellulose).

The TGA thermogram of CuO and CuO-C is shown in Fig. 5(b). For pure CuO, minimal weight loss was observed, indicating high thermal stability. The CuO-C exhibited a more pronounced weight loss, particularly in the temperature range of 200 to 400°C, which can be attributed to the thermal decomposition of the residual waste-derived cellulose. The initial weight loss below 200 °C for both samples corresponded to the removal of adsorbed moisture and surface hydroxyl groups (Apaydin Varol and Mutlu 2023). The CuO-C showed a residual weight loss at higher temperatures compared to pure CuO, suggesting that the residual cellulose underwent degradation, forming stable char residues.

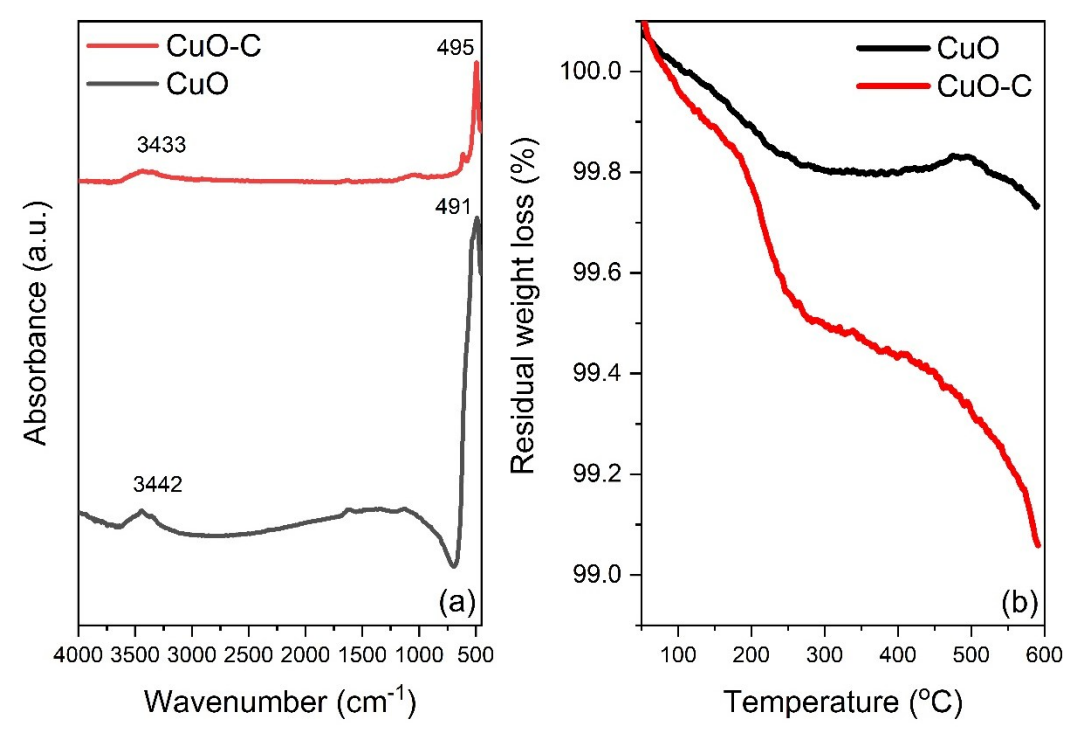


Fig. 5. (a) FTIR spectra and (b) TGA thermogram of the CuO and CuO-C

The SEM micrographs of CuO and CuO-C at varying magnifications are shown in Fig. 6. For CuO (Fig. 6a and 6b), a compact and aggregated morphology was observed, with densely packed NPs forming irregular clusters (Chan *et al.* 2022). The NP size is consistent with the crystallite size estimated from XRD analysis, confirming the nanoscale structure of the CuO material. In contrast, the CuO-C (Fig. 6c and 6d) exhibited a more dispersed and fibrous morphology. The waste-derived cellulose acts as a support structure, facilitating uniform distribution of CuO NPs and preventing their agglomeration. This morphology enhances the surface area and accessibility of active sites, corroborating the results of the nitrogen adsorption-desorption isotherms. The unique fibrous architecture of the CuO-C obtained suggests the role of waste-derived cellulose as a morphology tuner.

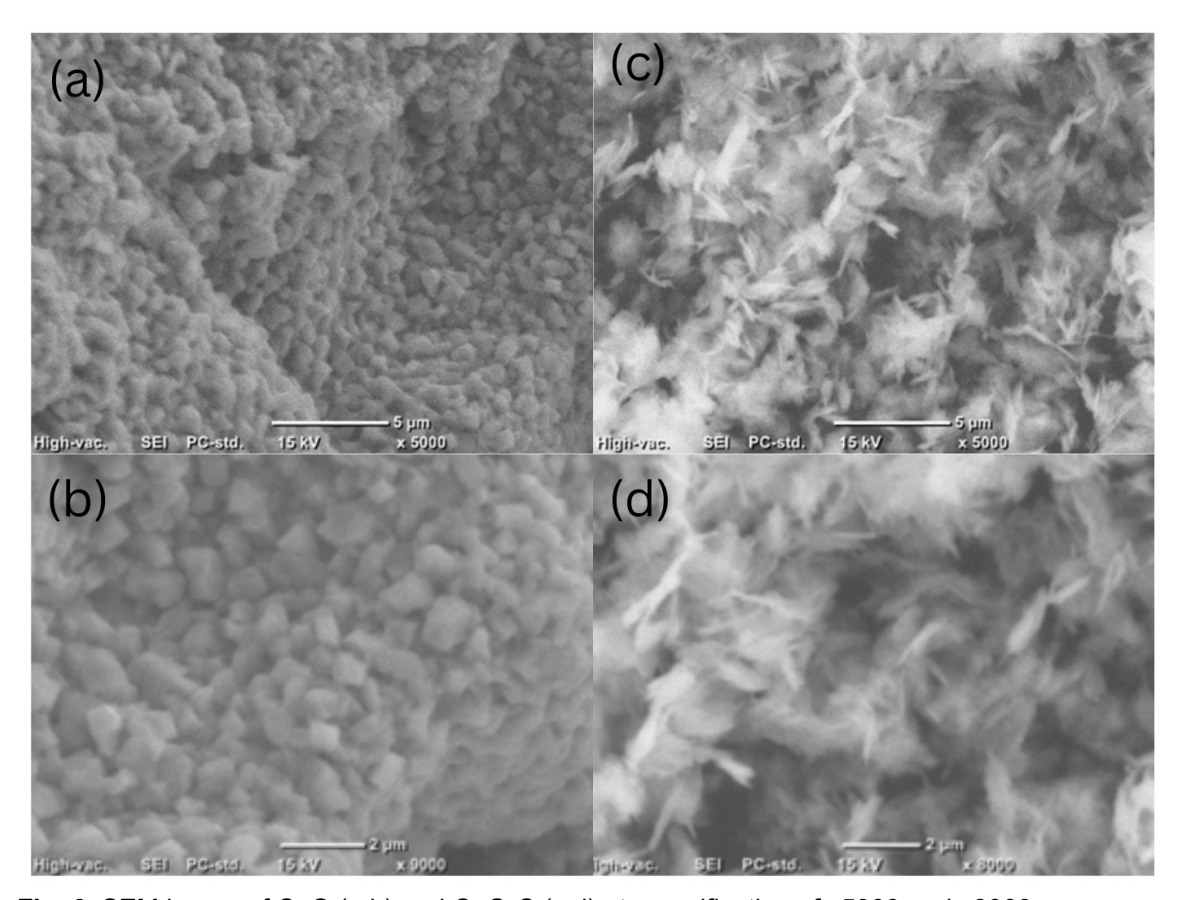


Fig. 6. SEM image of CuO (a,b) and CuO-C (c,d) at magnification of x5000 and x9000

The elemental composition of the CuO and CuO-C samples was investigated using EDX analysis, as shown in Fig. 7. For the pure CuO (Fig. 7a), the EDX spectrum revealed only Cu (72.52 at.%) and O (27.48 at.%), which is consistent with stoichiometric CuO. For the CuO-C (Fig. 7b), Cu (30.67 at.%) and O (51.44 at.%) remained dominant, with a detectable C signal (17.15 at.%) attributed to surface-adsorbed carbonaceous fragments, which likely originating from residual organics during cellulose-templated synthesis. Trace Cl (0.74 at.%) was also detected, possibly from the precursor salt. These results confirm that cellulose acted as a structural modulator, improving particle dispersion and porosity, but was not preserved as a bulk component in the final thermally treated CuO-C.

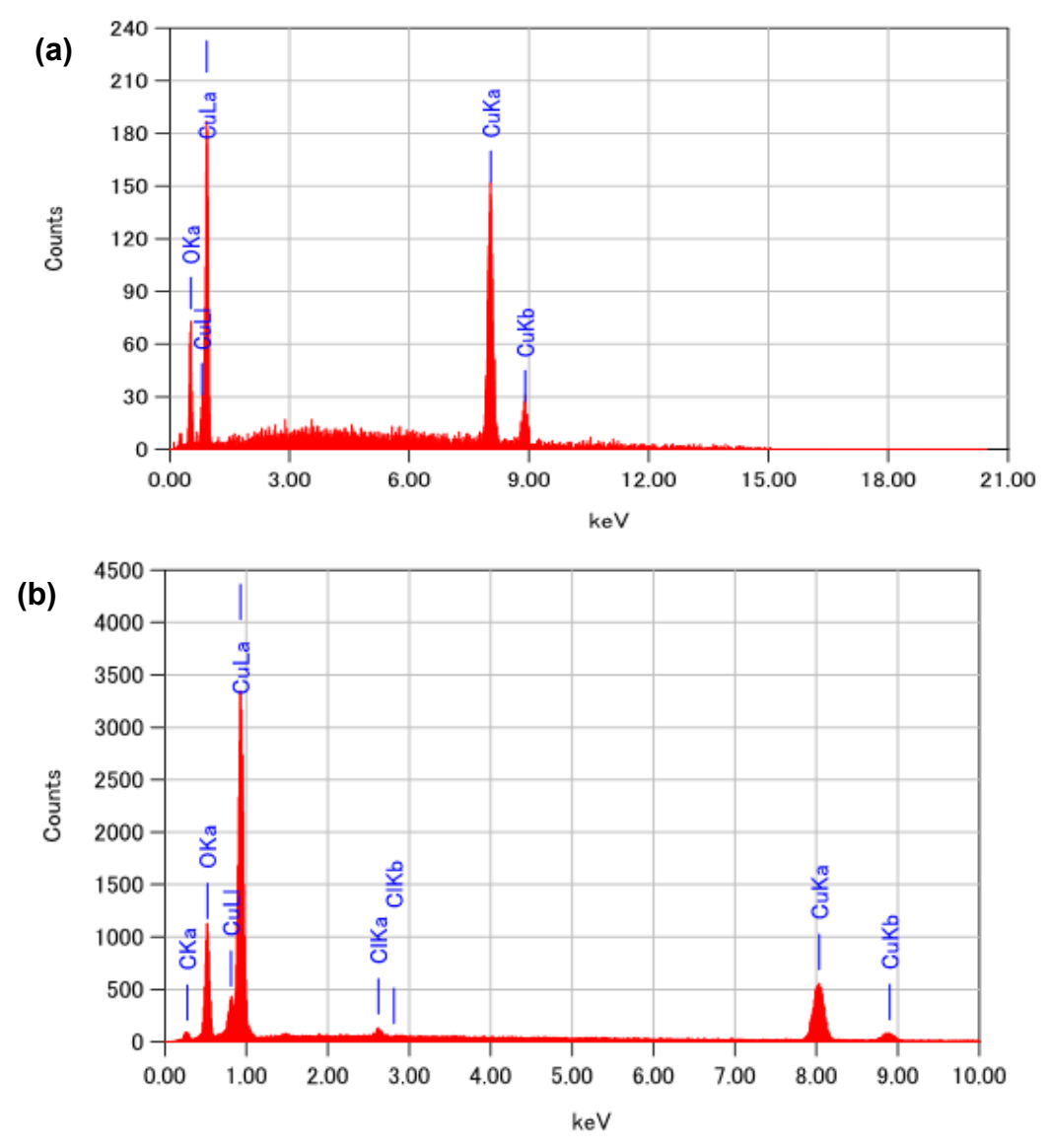


Fig. 7. Elemental composition of the synthesized (a) CuO and (b) CuO-C was analyzed using energy-dispersive X-ray (EDX) spectroscopy

The catalytic performance of CuO and CuO-C is shown in Fig. 8. The UV-Vis absorption spectrum (Fig. 8(a)) showed a significant decrease in the 4-NP peak at 400 nm and the appearance of a new peak at 300 nm, corresponding to 4-AP, upon catalytic reduction (Banou *et al.* 2023). The stepwise reduction process using CuO-C is shown in Fig. 8(b), where the gradual decrease of the 4-NP peak and the concurrent increase of the 4-AP peak confirm the efficient catalytic conversion. The time-dependent reduction profiles (Fig. 8b) demonstrate that CuO-C exhibited superior catalytic activity compared to pure CuO and the control without any catalyst. The C/C₀ ratio for 4-NP decreased more rapidly in the presence of CuO-C, with nearly complete conversion achieved within 15 min. In contrast, CuO required a longer reaction time to reach the same level of reduction, while the absence of a catalyst resulted in negligible conversion. This highlights the enhanced catalytic efficiency of CuO-C, which was likely due to its higher surface area and improved electron transfer capabilities.

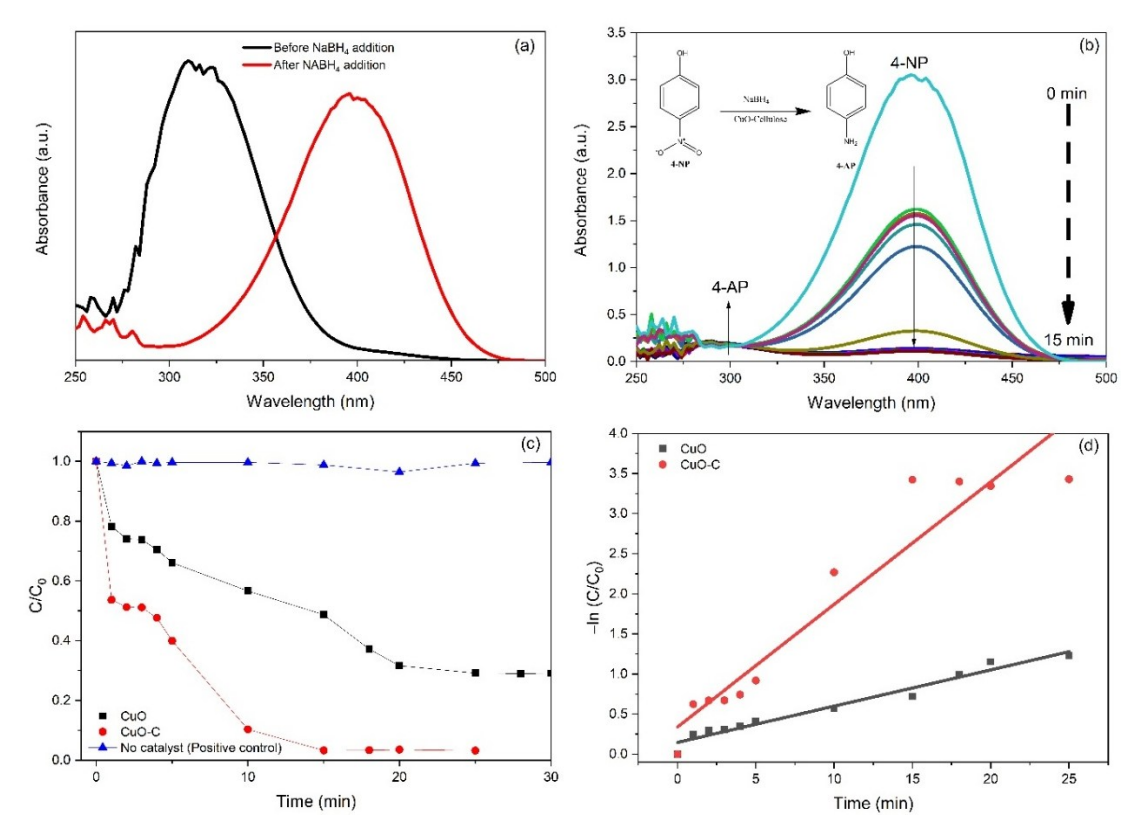


Fig. 8. (a) UV-Vis absorption spectra of 4-NP to 4-AP in the presence of NaBH₄; (b) Absorption spectra of 4-NP to 4-AP using CuO-C as catalyst; (c) Time dependent reduction profile; (d) Pseudo-first-order kinetic plots of 4-NP reduction using CuO and CuO-C

To quantify the catalytic efficiency of the samples, pseudo-first-order rate constants $(k_{\rm app})$ were determined using the linearized form of $-\ln(C/C_0)$ versus time for the 4-NP reduction, as shown in Fig. 8(d). The CuO-C exhibited a $k_{\rm app}$ of 0.153 min⁻¹, which was approximately 2.72 times higher than that of pure CuO (0.0563 min⁻¹). This enhanced catalytic efficiency is consistent with the BET results, where CuO-C displayed a markedly larger surface area (32 m²/g) compared to CuO (7 m²/g), providing more accessible active sites and improved electron transfer during the reduction process. These results highlight the potential of CuO-C as a highly efficient catalyst for environmental and industrial applications, particularly in pollutant remediation and fine chemical synthesis.

The antibacterial results demonstrated distinct differences in efficacy among the samples as shown in Fig. 9. For *S. aureus*, the CuO exhibited partial inhibition, with visible bacterial colonies reduced compared to the control. In contrast, the CuO-C demonstrated enhanced antibacterial activity, with negligible to no bacterial growth observed even at lower concentrations (x1 to x3 dilutions). This enhanced activity is likely attributable to the synergistic effects of CuO NPs, which generate reactive oxygen species (ROS), combined with their high surface area and improved interaction with bacterial cell walls (Khairy *et al.* 2024). A similar trend was observed for *K. pneumoniae*, where CuO only showed weak antibacterial activity. CuO-C, however, completely inhibited bacterial growth at higher concentrations (x1 to x2 dilutions) and only showed minimal growth at the lowest concentration (x4 dilution). In comparison, the control sample showed robust bacterial growth across all dilutions, confirming the lack of antibacterial activity of ethylene glycol.

Interestingly, the antibacterial activity was more pronounced against *S. aureus* than *K. pneumoniae*. This difference is likely due to the structural differences in the bacterial cell walls. *S. aureus*, a Gram-positive bacterium, has a thick peptidoglycan layer that is more permeable to reactive oxygen species and metal ions. In contrast, *K. pneumoniae*, a Gram-negative bacterium, has an additional outer membrane that limits the penetration of antibacterial agents and provides greater resistance (Banou *et al.* 2023; Slavin *et al.* 2017). The combination of ROS production from CuO-C and physical disruption (feather-like morphology) contributes to its enhanced bactericidal efficacy. These findings suggest that CuO-C is a promising candidate for antibacterial applications in biomedical coatings, food packaging, and water treatment, offering an eco-friendly and effective alternative to traditional antibacterial agents.

To contextualize the antibacterial performance of CuO-C, a comparison with previously reported CuO-based materials is presented in Table 3.

Table 3. Comparison of Antibacterial Activity of CuO-C with Previously Reported CuO-based Materials

Material	Bacterial Strain	Method	Performance	Reference
CuO	S. aureus	MIC (broth)	0.625 mg/mL	(Martínez-Corona et al. 2025)
CuO by Opuntia ficus indica	S. aureus	MIC (broth)	0.300 mg/mL	(Soliman and Salem 2025)
CuO (microwave- biogenic) by Lepidum sativum L. extract	S. aureus	MIC (broth)	0.075 mg/mL	(Ibrahim 2025)
CuO (microwave- biogenic) by Lepidum sativum L. extract	K. pneumoniae	MIC (broth)	0.075 mg/mL	(Ibrahim 2025)
CuO by Aegle marmelos extract	S. aureus	Disk diffusion	13 mm	(Thirunavukkarasu et al. 2025)
CuO NPs by ethanolic Neem extract	S. aureus	Disk diffusion	32 ± 2.12 mm	(Khairy <i>et al.</i> 2024)
CuO NPs by Jojoba extracts	S. aureus	Disk diffusion	28 ± 2.12 mm	(Khairy <i>et al.</i> 2024)
CuO NPs by Moringa Oleifera leaf extract	S. aureus	Disk diffusion	8 mm	(Bai <i>et al.</i> 2022)
CuO NPs (mechanochemical)	S. aureus	Disk diffusion	11.3–12.4 mm	(Ngamsurach and Praipipat 2022)
CuO-C	S. aureus	Spot test	10 ⁶ CFU/mL (total inhibition)	This work
CuO-C	K. pneumoniae	Spot test	10 ⁶ CFU/mL (total inhibition)	This work

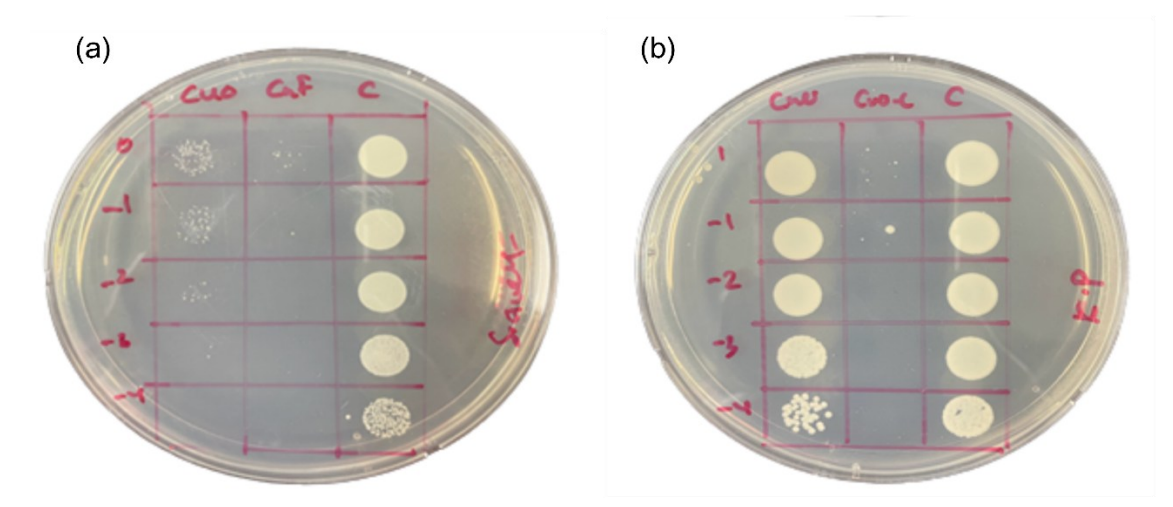


Fig. 9. Antibacterial test on (a) *Staphylococcus aureus* and (b) *Klebsiella pneumoniae* using CuO, CuO-C and control (ethylene glycol)

To evaluate the economic feasibility of the CuO-C, a cost analysis was performed based on the materials and processes used. The waste-derived cellulose was sourced as a byproduct from dissolution of cellulose process, making it cost-free. Other materials, such as CuSO₄·5H₂O, NaOH, and ethanol, were included in the cost assessment. The analysis also accounted for energy consumption during the drying and thermal treatment steps. The total cost of producing CuO-C was approximately RM 3.30 per gram, assuming similar preparation conditions for both materials. The negligible cost of waste-derived cellulose significantly reduces the overall expense of CuO-C synthesis compared to other potential additives. The cost analysis highlights the economic advantage of utilizing waste-derived cellulose for the synthesis of CuO-C. Moreover, the energy consumption during thermal treatment represents a significant portion of the total cost, suggesting potential optimization strategies for further cost reduction in future studies. Table 4 highlights the cost estimation for CuO-C preparation.

Table 4. Cost Analysis for the Synthesis of CuO and CuO-C

Item	Quantity	Unit Cost (RM)	Total Cost (RM)	Remarks
Raw Materials				
CuSO ₄ ·5H ₂ O	2.5 g	88.00/1 kg	0.22	Used for CuO precursor
NaOH	8.8 g	106.00/1 kg	0.93	Base for reaction
Ethanol	10 mL	225.00/2.5 L	0.90	Used for washing of CuO and CuO-C
Waste-derived cellulose* (Bamboo Biomass)	-	-	0.00	Repurposed from the dissolution of cellulose
Total Chemical cost			2.05	
Synthesis Costs				
Oven Drying (70 °C)	1.5 kWh X 24 h = 36 kWh	RM 0.39 per kWh**	14.04	Post-reaction drying
Thermal treatment	1.8 kWh X 2	RM 0.39 per	1.40	High-temperature
(500 °C)	h = 3.6 kWh	kWh**	1.40	treatment
Total Synthesis cost			15.44	
Total Cost of Goods Sold			17.49	Synthesis of 5.3 g of CuO

CONCLUSIONS

- 1. The incorporation of a highly alkaline solution from the cellulose extraction process into the precipitation synthesis of CuO enhanced both its structural and catalytic properties.
- 2. Additionally, the use of waste-derived cellulose also minimizes potential concerns related to nanoparticle leaching in practical applications. Thus, the cellulose-templated approach offers a dual benefit of promoting sustainability while improving the functional integrity of CuO-based materials.
- 3. CuO-C exhibited superior catalytic performance, achieving complete conversion of 4-NP to 4-AP within 15 min due to improved electron transfer and reactant adsorption.
- 4. The use of waste-derived cellulose as an additive not only aligns with principles of sustainability and circular economy but also substantially reduced material synthesis costs, with CuO-C costing RM 17.49 per batch, demonstrating its economic feasibility for scalable production.
- 5. BET surface area analysis confirmed a significant increase in specific surface area, from 7 m²/g for pure CuO to 32 m²/g for CuO-C, which contributed to enhanced catalytic efficiency.
- 6. The thermal treatment process effectively removed residual cellulosic contents, ensuring the purity and structural stability of the synthesized materials.
- 7. This study demonstrated the successful application of waste-derived cellulose, providing a cost-effective and environmentally responsible method for fabricating high performing CuO-based catalyst.
- 8. Future research should focus on optimizing synthesis parameters and investigating other waste-derived biomaterials, potentially broadening the applicability of such sustainable material in catalysis and environmental remediation.

ACKNOWLEDGMENTS

This work was supported by Universiti Putra Malaysia Grant GP-IPM/9750400. The authors confirm that there are no additional funders. The funder had no role in study design, data collection and analysis, decision to publish, or preparation of the manuscript. The authors acknowledged the anonymous reviewers for comments to improve the quality of this work.

REFERENCES CITED

Aggarwal, G., Chawla, S., Singh, A. J., Alampara, N., Monder, D. S., and Balasubramaniam, K. R. (2024). "Formation of an extended defect cluster in cuprous oxide," *Journal of Physics D: Applied Physics* 57(33), article 335103. DOI: 10.1088/1361-6463/ad4a82

Ajiz, H. A., Ardiansyah, R. P., Dwiatmaka, M. S. K. R., Setyawan, H., Nurtono, T., and Widiyastuti, W. (2024). "Silica surface modification using cellulose as a renewable

- organosilane derived from coconut coir fiber for carbon capture," *Results in Engineering* 24, article 103060. DOI: 10.1016/j.rineng.2024.103060
- Apaydın Varol, E., and Mutlu, Ü. (2023). "TGA-FTIR analysis of biomass samples based on the thermal decomposition behavior of hemicellulose, cellulose, and lignin," *Energies* 16(9), article 3674. DOI: 10.3390/en16093674
- Asmare, Z. G., Aragaw, B. A., and Atlabachew, M. (2024). "Facile synthesis of natural kaolin-based CuO catalyst: An efficient heterogeneous catalyst for the catalytic reduction of 4-nitrophenol," *ACS Omega* 9(49), 48014-48031. DOI: 10.1021/acsomega.4c04029
- Bai, B., Saranya, S., Dheepaasri, V., Muniasamy, S., Alharbi, N. S., Selvaraj, B., Undal, V. S., and Gnanamangai, B. M. (2022). "Biosynthesized copper oxide nanoparticles (CuO NPs) enhances the anti-biofilm efficacy against *K. pneumoniae* and *S. aureus*," *Journal of King Saud University Science* 34(6), article 102120. DOI: 10.1016/j.jksus.2022.102120
- Banou, M., Niu, Y., Ammari, F., Dunlop, T., Palmer, R. E., and Tizaoui, C. (2023). "Fabrication of graphene nanoplatelets/MgAl-layered double hydroxide nanocomposites as efficient support for gold nanoparticles and their catalytic performance in 4-nitrophenol reduction," *Process Safety and Environmental Protection* 174, 891-900. DOI: 10.1016/j.psep.2023.04.051
- Bekru, A. G., Zelekew, O. A., Andoshe, D. M., Sabir, F. K., and Eswaramoorthy, R. (2021). "Microwave-assisted synthesis of CuO nanoparticles using *Cordia africana* Lam. leaf extract for 4-nitrophenol reduction," *Journal of Nanotechnology* 2021, 1-12. DOI: 10.1155/2021/5581621
- Bhaskar, M, P., Nair, S., and Santhanagopalan, D. (2024). "Cobalt-free CuO catalyst for hydrolytic dehydrogenation of sodium borohydride and ammonia borane," *International Journal of Hydrogen Energy* 51, 551-561. DOI: 10.1016/j.ijhydene.2023.08.260
- Bhat, N., Ukkund, S. J., Ashraf, M., Acharya, K., J. Ramegouda, N., Puthiyillam, P., Hasan, M. A., Islam, S., Koradoor, V. B., Praveen, A. D., and Khan, M. A. (2023). "GO/CuO nanohybrid-based carbon dioxide gas sensors with an Arduino detection unit," *ACS Omega* 8(36), 32512-32519. DOI: 10.1021/acsomega.3c02598
- Chakrabarty, S., Tamim, A., Yılmaz, M., Dhar, P. K., Mim, R. M., and Dutta, S. K. (2023). "Adsorption of Pb (II) ions from aqueous solution using CuO-ZnO nanocomposites," *Chemistry Africa* 6(3), 1449-1462. DOI: 10.1007/s42250-022-00554-7
- Chan, Y., Selvanathan, V., Tey, L.-H., Akhtaruzzaman, Md., Anur, F., Djearamane, S., Watanabe, A., and Aminuzzaman, M. (2022). "Effect of calcination temperature on structural, morphological and optical properties of copper oxide nanostructures derived from *Garcinia mangostana* L. leaf extract," *Nanomaterials* 12(20), article 3589. DOI: 10.3390/nano12203589
- Devaraji, M., Thanikachalam, P. V., and Elumalai, K. (2024). "The potential of copper oxide nanoparticles in nanomedicine: A comprehensive review," *Biotechnology Notes* 5, 80-99. DOI: 10.1016/j.biotno.2024.06.001
- Ehsani, A., Nejatbakhsh, S., Soodmand, A. M., Farshchi, M. E., and Aghdasinia, H. (2023). "High-performance catalytic reduction of 4-nitrophenol to 4-aminophenol using M-BDC (M = Ag, Co, Cr, Mn, and Zr) metal-organic frameworks," *Environmental Research* 227, article 115736. DOI: 10.1016/j.envres.2023.115736
- Hong, J., Li, J., and Ni, Y. (2009). "Urchin-like CuO microspheres: Synthesis,

- characterization, and properties," *Journal of Alloys and Compounds* 481(1-2), 610-615. DOI: 10.1016/j.jallcom.2009.03.043
- Ibrahim, A. A. (2025). "Microwave-assisted biogenic synthesis of pure copper oxide nanoparticles by Lepidium sativum L. leaves extract: Characterization and evaluation of antibacterial activity," *Journal of Biotechnology* 406, 82-90. DOI: 10.1016/j.jbiotec.2025.07.003
- Jadbabaei, N., Slobodjian, R. J., Shuai, D., and Zhang, H. (2017). "Catalytic reduction of 4-nitrophenol by palladium-resin composites," *Applied Catalysis A: General* 543, 209-217. DOI: 10.1016/j.apcata.2017.06.023
- Kassie, B. B., Daget, T. M., and Tassew, D. F. (2024). "Synthesis, functionalization, and commercial application of cellulose-based nanomaterials," *International Journal of Biological Macromolecules* 278, article 134990. DOI: 10.1016/j.ijbiomac.2024.134990
- Kästner, C., and Thünemann, A. F. (2016). "Catalytic reduction of 4-nitrophenol using silver nanoparticles with adjustable activity," *Langmuir* 32(29), 7383-7391. DOI: 10.1021/acs.langmuir.6b01477
- Khairy, T., Amin, D. H., Salama, H. M., Elkholy, I. M. A., Elnakib, M., Gebreel, H. M., and Sayed, H. A. E. (2024). "Antibacterial activity of green synthesized copper oxide nanoparticles against multidrug-resistant bacteria," *Scientific Reports* 14(1), article 25020. DOI: 10.1038/s41598-024-75147-0
- Koniakhin, S. V., Utesov, O. I., and Yashenkin, A. G. (2024). "Raman peak shift and broadening in crystalline nanoparticles with lattice impurities," *Diamond and Related Materials* 146, article 111182. DOI: 10.1016/j.diamond.2024.111182
- Li, M., Ding, C., Jia, P., Guo, L., Wang, S., Guo, Z., Su, F., and Huang, Y. (2021). "Semi-quantitative detection of p-Aminophenol in real samples with colorfully naked-eye assay," *Sensors and Actuators B: Chemical* 334, article 129604. DOI: 10.1016/j.snb.2021.129604
- Li, X., Li, G., Zang, W., Wang, L., and Zhang, X. (2014). "Catalytic activity of shaped platinum nanoparticles for hydrogenation: A kinetic study," *Catalysis Science & Technology* 4(9), article 3290. DOI: 10.1039/C4CY00580E
- Martínez-Corona, Z., García-Zaleta, D. S., López-González, R., García-Mendoza, C., Alvarez-Lemus, M. A., Encarnacion-Gomez, C., and Gómez-Cornelio, S. A. (2025). "Antibacterial activity of TiO₂, CuO, and CuO/TiO₂ nanomaterials and their potential application on construction surfaces," *Journal of Materials Science: Materials in Engineering* 20(1), 70. DOI: 10.1186/s40712-025-00288-7
- Mekhzoum, M. E. M., El Bourakadi, K., Qaiss, A. el K., and Bouhfid, R. (2021). "Cellulose nanocrystal/nanoparticles hybrid nanocomposites: From preparation to applications," in: *Cellulose Nanocrystal/Nanoparticles Hybrid Nanocomposites*, Elsevier, 1-25. DOI: 10.1016/B978-0-12-822906-4.00008-6
- Menumerov, E., Hughes, R. A., and Neretina, S. (2016). "Catalytic reduction of 4-nitrophenol: A quantitative assessment of the role of dissolved oxygen in determining the induction time," *Nano Letters* 16(12), 7791-7797. DOI: 10.1021/acs.nanolett.6b03991
- Mistry, K., Snowden, H., Darling, G. R., and Hodgson, A. (2024). "Hydroxyl on stepped copper and its interaction with water," *The Journal of Physical Chemistry C* 128(31), 13025-13033. DOI: 10.1021/acs.jpcc.4c04091
- Naz, S., Gul, A., Zia, M., and Javed, R. (2023). "Synthesis, biomedical applications, and toxicity of CuO nanoparticles," *Applied Microbiology and Biotechnology* 107(4),

- 1039-1061. DOI: 10.1007/s00253-023-12364-z
- Nazim, M., Khan, A. A. P., Asiri, A. M., and Kim, J. H. (2021). "Exploring rapid photocatalytic degradation of organic pollutants with porous CuO nanosheets: Synthesis, dye removal, and kinetic studies at room temperature," *ACS Omega* 6(4), 2601-2612. DOI: 10.1021/acsomega.0c04747
- Neal, R. D., Inoue, Y., Hughes, R. A., and Neretina, S. (2019). "Catalytic reduction of 4-nitrophenol by gold catalysts: The influence of borohydride concentration on the induction time," *The Journal of Physical Chemistry C* 123(20), 12894-12901. DOI: 10.1021/acs.jpcc.9b02396
- Ngamsurach, P., and Praipipat, P. (2022). "Antibacterial activities against *Staphylococcus aureus* and *Escherichia coli* of extracted *Piper betle* leaf materials by disc diffusion assay and batch experiments," *RSC Advances* 12(40), 26435-26454. DOI: 10.1039/D2RA04611C
- Noël, S., Bricout, H., Addad, A., Sonnendecker, C., Zimmermann, W., Monflier, E., and Léger, B. (2020). "Catalytic reduction of 4-nitrophenol with gold nanoparticles stabilized by large-ring cyclodextrins," *New Journal of Chemistry* 44(48), 21007-21011. DOI: 10.1039/D0NJ03687K
- Panigrahy, N., Priyadarshini, A., Sahoo, M. M., Verma, A. K., Daverey, A., and Sahoo, N. K. (2022). "A comprehensive review on eco-toxicity and biodegradation of phenolics: Recent progress and future outlook," *Environmental Technology & Innovation* 27, article 102423. DOI: 10.1016/j.eti.2022.102423
- Peng, F., Sun, Y., Lu, Y., Yu, W., Ge, M., Shi, J., Cong, R., Hao, J., and Dai, N. (2020). "Studies on sensing properties and mechanism of CuO nanoparticles to H₂S gas," *Nanomaterials* 10(4), article 774. DOI: 10.3390/nano10040774
- Poreddy, R., Engelbrekt, C., and Riisager, A. (2015). "Copper oxide as efficient catalyst for oxidative dehydrogenation of alcohols with air," *Catalysis Science & Technology* 5(4), 2467-2477. DOI: 10.1039/C4CY01622J
- Raizada, P., Sudhaik, A., Patial, S., Hasija, V., Parwaz Khan, A. A., Singh, P., Gautam, S., Kaur, M., and Nguyen, V.-H. (2020). "Engineering nanostructures of CuO-based photocatalysts for water treatment: Current progress and future challenges," *Arabian Journal of Chemistry* 13(11), 8424-8457. DOI: 10.1016/j.arabjc.2020.06.031
- Saif, S., Adil, S. F., Khan, M., Hatshan, M. R., Khan, M., and Bashir, F. (2021). "Adsorption studies of arsenic(V) by CuO nanoparticles synthesized by *Phyllanthus emblica* leaf-extract-fueled solution combustion synthesis," *Sustainability* 13(4), articl e2017. DOI: 10.3390/su13042017
- Shimizu, S., and Matubayasi, N. (2024). "Sorption hysteresis: A statistical thermodynamic fluctuation theory," *Langmuir* 40(22), 11504-11515. DOI: 10.1021/acs.langmuir.4c00606
- Sibhatu, A. K., Weldegebrieal, G. K., Sagadevan, S., Tran, N. N., and Hessel, V. (2022). "Photocatalytic activity of CuO nanoparticles for organic and inorganic pollutants removal in wastewater remediation," *Chemosphere* 300, article 134623. DOI: 10.1016/j.chemosphere.2022.134623
- Slavin, Y. N., Asnis, J., Häfeli, U. O., and Bach, H. (2017). "Metal nanoparticles: Understanding the mechanisms behind antibacterial activity," *Journal of Nanobiotechnology* 15(1), article 65. DOI: 10.1186/s12951-017-0308-z
- Soliman, M. K. Y., and Salem, S. S. (2025). "Comparative evaluation of antimicrobial, antibiofilm, antioxidant, antiviral, and antidiabetic activities of copper oxide

- nanoparticles biofabricated via Opuntia ficus indica," *Scientific Reports* 15(1), article 24823. DOI: 10.1038/s41598-025-08878-3
- Steinhauer, S. (2021). "Gas sensors based on copper oxide nanomaterials: A review," *Chemosensors* 9(3), article 51. DOI: 10.3390/chemosensors9030051
- Su, C., Zhao, S., Wang, P., Chang, W., Chang, K., and Zhang, H. (2016). "Synthesis and characterization of ultrafined palladium nanoparticles decorated on 2D magnetic graphene oxide nanosheets and their application for catalytic reduction of 4-nitrophenol," *Journal of Environmental Chemical Engineering* 4(3), 3433-3440. DOI: 10.1016/j.jece.2016.07.021
- Sudhakar, P., and Soni, H. (2018). "Catalytic reduction of nitrophenols using silver nanoparticles-supported activated carbon derived from agro-waste," *Journal of Environmental Chemical Engineering* 6(1), 28-36. DOI: 10.1016/j.jece.2017.11.053
- Thirunavukkarasu, R., Nandhagopal, M., Thirunavukkarasu, S., Raji, A., Kamath, B. R., and Venkateswaran, L. (2025). "Ecosynthesis of copper and nickel oxide nanoparticles from *Aegle marmelos* extract: Antimicrobial, antioxidant, and hemolytic activity evaluation," *Materials Letters* 395, article 138705. DOI: 10.1016/j.matlet.2025.138705
- Tran, T. H., and Nguyen, V. T. (2014). "Copper oxide nanomaterials prepared by solution methods, some properties, and potential applications: A brief review," *International Scholarly Research Notices* 2014, 1-14. DOI: 10.1155/2014/856592
- Wang, F., Li, H., Yuan, Z., Sun, Y., Chang, F., Deng, H., Xie, L., and Li, H. (2016). "A highly sensitive gas sensor based on CuO nanoparticles synthetized via a sol-gel method," *RSC Advances* 6(83), 79343-79349. DOI: 10.1039/C6RA13876D
- Wang, W., Wang, L., Shi, H., and Liang, Y. (2012). "A room temperature chemical route for large scale synthesis of sub-15 nm ultralong CuO nanowires with strong size effect and enhanced photocatalytic activity," *CrystEngComm* 14(18), article 5914. DOI: 10.1039/c2ce25666e
- Warren, W. R., and LaJeunesse, D. R. (2019). "Characterization of hydrothermal deposition of copper oxide nanoleaves on never-dried bacterial cellulose," *Polymers* 11(11), article 1762. DOI: 10.3390/polym11111762
- Xu, J. F., Ji, W., Shen, Z. X., Tang, S. H., Ye, X. R., Jia, D. Z., and Yin, X. Q. (1999). "Synthesis and Raman spectra of cupric oxide quantum dots," *MRS Proceedings* 571, article 229. DOI: 10.1557/PROC-571-229
- Xu, C., Qiu, Y., Yang, X., Gao, Z., Wang, Z., Liu, C., Sun, Y., Ma, J., and Liu, L. (2024a). "High-performance catalytic reduction of 4-nitrophenol to 4-aminophenol over Pt nanoparticles supported on Co-Al LDH nanosheets," *Crystals* 14(3), article 284. DOI: 10.3390/cryst14030284
- Xu, R., Su, Y., Ji, H., Jiang, M., Zhang, R., Ding, L., Chen, Y., and Song, D. (2024b). "Enhanced detection of 4-nitrophenol in drinking water: ECL sensor utilizing velvet-like graphitic carbon nitride and molecular imprinting," *Food Chemistry* 460, article 140599. DOI: 10.1016/j.foodchem.2024.140599
- Zedan, A. F., Mohamed, A. T., El-Shall, M. S., AlQaradawi, S. Y., and AlJaber, A. S. (2018). "Tailoring the reducibility and catalytic activity of CuO nanoparticles for low temperature CO oxidation," *RSC Advances* 8(35), 19499-19511. DOI: 10.1039/C8RA03623C
- Zhao, B., Mele, G., Pio, I., Li, J., Palmisano, L., and Vasapollo, G. (2010). "Degradation of 4-nitrophenol (4-NP) using Fe-TiO2 as a heterogeneous photo-Fenton catalyst," *Journal of Hazardous Materials* 176(1-3), 569-574. DOI:

- 10.1016/j.jhazmat.2009.11.066
- Zheng, A. L. T., Sabidi, S., Ohno, T., Maeda, T., and Andou, Y. (2022). "Cu₂O/TiO₂ decorated on cellulose nanofiber/reduced graphene hydrogel for enhanced photocatalytic activity and its antibacterial applications," *Chemosphere* 286, article e131731. DOI: 10.1016/j.chemosphere.2021.131731
- Zheng, A. L. T., Teo, E. Y. L., Seenivasagam, S., Yiu, P. H., Boonyuen, S., Chung, E. L. T., Lease, J., and Andou, Y. (2024). "Nanostructures embedded on porous materials for the catalytic reduction of nitrophenols: A concise review," *Journal of Porous Materials* 31(5), 1557-1575. DOI: 10.1007/s10934-024-01618-4
- Zhou, Z., Lu, C., Wu, X., and Zhang, X. (2013). "Cellulose nanocrystals as a novel support for CuO nanoparticles catalysts: Facile synthesis and their application to 4-nitrophenol reduction," *RSC Advances* 3(48), article 26066. DOI: 10.1039/c3ra43006e

Article submitted: May 29, 2025; Peer review completed: July 1, 2025; Revised version received: August 1, 2025; Accepted: August 2, 2025; Published: August 28, 2025. DOI: 10.15376/biores.20.4.9148-9166